

Sequential Pulses of Apical Epithelial Secretion and Endocytosis Drive Airway Maturation in *Drosophila*

Vasilios Tsarouhas,^{1,2} Kirsten-André Senti,^{1,2} Satish Arcot Jayaram,¹ Katarína Tiklová,¹ Johanna Hemphälä,¹ Jeremy Adler,¹ and Christos Samakovlis^{1,*}

¹ Wenner-Gren Institute, Stockholm University, Department of Developmental Biology, Svante Arrheniusväg 16, Arrheniuslab E3, S-10691 Stockholm, Sweden

² These authors contributed equally to this work.

*Correspondence: christos@devbio.su.se

DOI 10.1016/j.devcel.2007.06.008

SUMMARY

The development of air-filled respiratory organs is crucial for survival at birth. We used a combination of live imaging and genetic analysis to dissect respiratory organ maturation in the embryonic *Drosophila* trachea. We found that tracheal tube maturation entails three precise epithelial transitions. Initially, a secretion burst deposits proteins into the lumen. Solid luminal material is then rapidly cleared from the tubes, and shortly thereafter liquid is removed. To elucidate the cellular mechanisms behind these transitions, we identified gas-filling-deficient mutants showing narrow or protein-clogged tubes. These mutations either disrupt endoplasmic reticulum-to-Golgi vesicle transport or endocytosis. First, Sar1 is required for protein secretion, luminal matrix assembly, and diametric tube expansion. Subsequently, a sharp pulse of Rab5-dependent endocytic activity rapidly internalizes and clears luminal contents. The coordination of luminal matrix secretion and endocytosis may be a general mechanism in tubular organ morphogenesis and maturation.

INTRODUCTION

Branched tubular organs are essential for oxygen and nutrient transport. Such organs include the blood circulatory system, the lung and kidney in mammals, and the tracheal respiratory system in insects. The optimal flow of transported fluids depends on the uniform length and diameter of the constituting tubes in the network. Alterations in the distinct tube shapes and sizes cause pronounced defects in animal physiology and lead to serious pathological conditions. For example, tube overgrowth and cyst formation in the collecting duct are intimately linked to the pathology of Autosomal Dominant

Polycystic Kidney Disease. Conversely, stenoses, the abnormal narrowing of blood vessels and other tubular organs, are associated with ischemias and organ obstructions (Lubarsky and Krasnow, 2003; Sadler, 1985).

While the early steps of differentiation, lumen formation, and branch patterning begin to be elucidated in several tubular organs (Affolter et al., 2003; Hogan and Kolodziej, 2002), we only have scarce glimpses into the cellular events of lumen expansion and tubular organ maturation. De novo lumen formation can be induced in three-dimensional cultures of MDCK cells. Recent studies in this system revealed that PTEN activation, apical cell membrane polarization, and Cdc42 activation are key events in lumen formation in vitro (Martin-Belmonte et al., 2007). In zebrafish embryos and cultured human endothelial cells, capillary vessels form through the coalescence and growth of intracellular pinocytotic vesicles (Kamei et al., 2006). These tubular vacuoles then fuse with the plasma membranes to form a continuous extracellular lumen. Salivary gland extension in *Drosophila* requires the transcriptional upregulation of the apical membrane determinant Crumbs (Crb) (Myat and Andrew, 2002), but the cellular mechanism leading to gland expansion remains unclear.

The epithelial cells of the *Drosophila* tracheal network form tubes of different sizes and cellular architecture, and they provide a genetically amenable system for the investigation of branched tubular organ morphogenesis. Tracheal development begins during the second half of embryogenesis when 20 metameric placodes invaginate from the epidermis. Through a series of stereotypic branching and fusion events, the tracheal epithelial cells generate a tubular network extending branches to all embryonic tissues. In contrast to the wealth of knowledge about tracheal patterning and branching (Ghabrial et al., 2003; Uv et al., 2003), the later events of morphogenesis and tube maturation into functional airways have yet to be elucidated. As the nascent, liquid-filled tracheal network develops, the epithelial cells deposit an apical chitinous matrix into the lumen. The assembly of this intraluminal polysaccharide cable coordinates uniform tube growth (reviewed by Swanson and Beitel, 2006). Two luminal, putative chitin deacetylases, Vermiform (Verm) and Serpentine (Serp), are selectively required for termination of

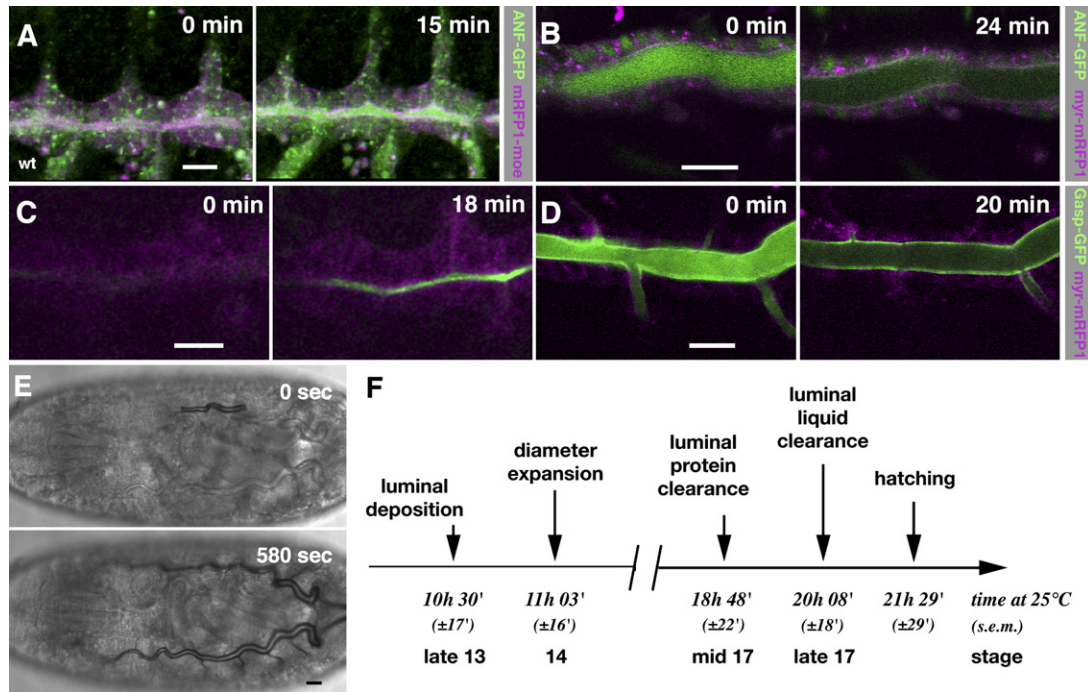


Figure 1. Identification of Four Distinct Events in Tracheal Tube Maturation

(A and B) Selected images from two time-lapse confocal movies of live wild-type *btl* > ANF-GFP embryos showing the (A) luminal deposition burst of ANF-GFP at 10.5 hr after egg laying (AEL) and the (B) luminal ANF-GFP clearance at 19 hr (green) (Movies S1 and S2).

(C and D) (C) Deposition and (D) clearance of Gasp-GFP in *btl* > Gasp-GFP embryos (green) (Movies S3 and S4).

(E) Two selected images from a wide-field movie illustrating the liquid clearance/gas filling of a wild-type embryo. The upper panel shows initiation of the gas filling (first gas bubble), while the lower panel shows its completion, when all tracheal branches are gas filled (Movie S5).

(F) Summary of recordings showing the maturation events of embryos expressing *btl* > ANF-GFP in real time (n = 237).

Tracheal cells were marked by the (A) *btl*-mRFP1-*moe* or (B–D) *btl* > *myr*-mRFP1 transgenes (magenta). SEM denotes the standard error of means. Scale bars are 10 μ m in (A)–(D) and 20 μ m in (E).

branch elongation. The analysis of *verm* and *serp* mutants indicates that modifications in the rigidity of the matrix are sensed by the surrounding epithelium to restrict tube length (Luschnig et al., 2006; Wang et al., 2006). What drives the diametric expansion of the emerging narrow branches to their final size? How are the matrix- and liquid-filled tracheal tubes cleared at the end of embryogenesis?

Here, we use live imaging of secreted GFP-tagged proteins to identify the cellular mechanisms transforming the tracheal tubes into a functional respiratory organ. We characterize the precise sequence and cellular dynamics of a secretory and an endocytic pulse that precede the rapid liquid clearance and gas filling of the network. Analysis of mutants with defects in gas filling reveals three distinct but functionally connected steps of airway maturation. Sar1-mediated luminal deposition of secreted proteins is tightly coupled with the expansion of the intraluminal matrix and tube diameter. Subsequently, a Rab5-dependent endocytotic wave frees the lumen of solid material within 30 min. We show that the precise coordination of secretory and endocytotic activities first direct tube diameter growth and then ensure lumen clearance to generate functional airways.

RESULTS

Live Imaging of Airway Maturation

We established a live-imaging approach to analyze the maturation of the *Drosophila* tracheal network. Using *btl*-GAL4, we coexpressed heterologous or endogenous GFP-tagged secreted molecules along with cytoplasmic RFP reporters to label tracheal cells (Shiga et al., 1996). Live embryos were then imaged by wide-field or confocal microscopy.

ANF-GFP (rat Atrial Natriuretic Factor fused to GFP) serves as a functionally inert, heterologous secretion marker in *Drosophila* (Rao et al., 2001). We recorded the development of the dorsal trunk (DT) of embryos expressing *btl* > ANF-GFP (*btl*-GAL4 UAS-ANF-GFP) and *btl*-RFP-*moesin* (*moe*) (Ribeiro et al., 2004) to visualize tracheal cells (Figure 1A; see Movie S1 in the Supplemental Data available with this article online). Initially, during early stage 13, ANF-GFP predominantly localized in the cytoplasm, and the apical concentration of RFP-*moe* demarcated the narrow lumen of the nascent tracheal tubes. In a sudden burst, ANF-GFP was deposited into the lumen, and its luminal levels increased abruptly within 15 min. As luminal secretion continued, cytoplasmic ANF-GFP

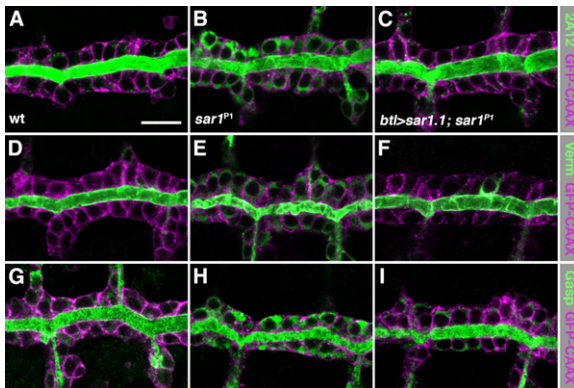


Figure 2. *sar1* Is Required for Efficient Luminal Secretion of Proteins

(A–I) Confocal sections of the DT of (A, D, and G) wild-type, (B, E, and H) the *sar1^{P1}* mutant, and (C, F, and I) *btl > sar1.1; sar1^{P1}* rescued embryos. All embryos expressed *btl > GFP-CAAX* (magenta). Embryos were stained for the luminal antigens (A–C) 2A12, (D–F) Verm, and (G–I) Gasp (green). *sar1^{P1}* mutant embryos show strong intracellular retention of luminal markers. Tracheal expression of *sar1* largely rescues the luminal secretion phenotype of *sar1^{P1}* mutant embryos. Scale bars are 10 μ m.

rapidly passed through dynamic, large vesicular structures. Half an hour after the secretion burst, tube diameter began to expand, shown by the RFP-moe labeling. By early stage 16, the ANF-GFP signal resided mostly in the lumen, and, concomitantly, diametric expansion ended. Thus, ANF-GFP reports a sudden luminal deposition event.

At stage 16, the DT lumen contains multiple proteins and a chitinous cable (Devine et al., 2005; Tonning et al., 2005). To follow the fate of the luminal proteins, we imaged embryos expressing ANF-GFP and the membrane marker myr-RFP in the trachea from stage 16 onward (Figure 1B; Movie S2). Initially, high levels of ANF-GFP filled the lumen. At mid-stage 17, luminal ANF-GFP rapidly declined within 24 min to very low levels. In contrast, the cytoplasmic ANF-GFP levels remained constant and low. Therefore, the dramatic drop in luminal ANF-GFP intensity highlights a wave of luminal protein clearance.

How does the dynamic ANF-GFP deposition and clearance relate to endogenous luminal markers? Live imaging of embryos expressing the luminal protein Gasp tagged to GFP (Barry et al., 1999) shows that Gasp-GFP first accumulates in the lumen and is then removed similarly to ANF-GFP (Figures 1C and 1D; Movies S3 and S4). The dynamic localization of GFP-tagged variants of Verm or Serp was identical (data not shown). Furthermore, analysis of fixed embryos shows that endogenous Verm and Gasp are first deposited and then cleared from the tracheal lumen very much like ANF-GFP (Figure S1). Finally, we fixed *btl > ANF-GFP* embryos at set times before and after the luminal ANF-GFP clearance (18 hr and 20 hr after egg laying [AEL]) for Transmission Electron Microscopy (TEM). Also, this assay showed that the luminal chitinous cable disappeared within the interval of ANF-GFP clear-

ance (Figure S1). Thus, ANF-GFP faithfully reports the rapid and massive deposition of endogenous luminal content at stage 13 and its complete removal at mid-stage 17.

To visualize the transition from liquid- to gas-filled trachea, we recorded late stage-17 embryos (Figure 1E; Movie S5). In a stereotypic sequence, a bubble of a so far unknown gas appears stochastically in one of the DT central metameres (4–6) and quickly expands first posteriorly and then anteriorly. The bubble then spreads through the posterior anastomosis to the contralateral DT, where it again rapidly extends anteriorly. Within 10 min, the entire tracheal tree fills with gas. Approximately 80 min later, the mature larva hatches.

To embed the single steps in a developmental framework, we recorded multiple embryos expressing *btl > ANF-GFP* and timed each of the morphological changes. All transitions occurred robustly within a defined, precise time interval (Figure 1F; Experimental Procedures).

Taken together, our live-imaging approach identifies three dramatic and dynamic changes in luminal morphology that divide tracheal maturation into precisely timed steps. A secretory burst deposits large quantities of luminal proteins into the tracheal lumen and tightly precedes tube diameter expansion. The tracheal epithelium then clears these proteins and liquid by two sequential pulse-like events generating functional, mature airways. What are the underlying cellular and molecular mechanisms executing the rapid transitions? What is the functional relevance of the transitions for airway maturation? We addressed those questions by analyzing mutants with defects in gas filling.

***sar1* Is Required for Efficient Secretion into the Tracheal Lumen**

We identified two strong, hypomorphic *sar1* alleles in screens for mutants with tracheal tube defects (see Experimental Procedures and Figure S2). *sar1* encodes a small GTPase that regulates COPII vesicle budding from the endoplasmic reticulum (ER) to the Golgi apparatus (reviewed in Bonifacino and Glick, 2004). In wild-type embryos, the bulk of luminal markers 2A12, Verm, and Gasp has been deposited inside the DT lumen by stage 15 (Figures 2A, 2D, and 2G). However, in zygotic *sar1^{P1}* mutants (hereafter referred to as *sar1*), luminal secretion of 2A12, Verm, and Gasp was incomplete. The tracheal cells outlined by GFP-CAAX partially retained those markers in the cytoplasm (Figures 2B, 2E, and 2H). *sar1* zygotic mutant embryos normally deposited the early luminal marker Piopio by stage 13 (Jazwinska et al., 2003). Luminal chitin was also detected in *sar1* mutants at stage 15. However, the luminal cable was narrow, more dense (Figure S3), and distorted compared to wild-type (Figures 3E and 3F). To test if the *sar1* secretory phenotype in the trachea is cell autonomous, we reexpressed Sar1 specifically in the trachea of *sar1* mutants by using *btl-GAL4*. Such embryos showed largely restored secretion of 2A12, Verm, and Gasp (Figures 2C, 2F, and 2I). Thus, we conclude that tracheal *sar1* is required for the

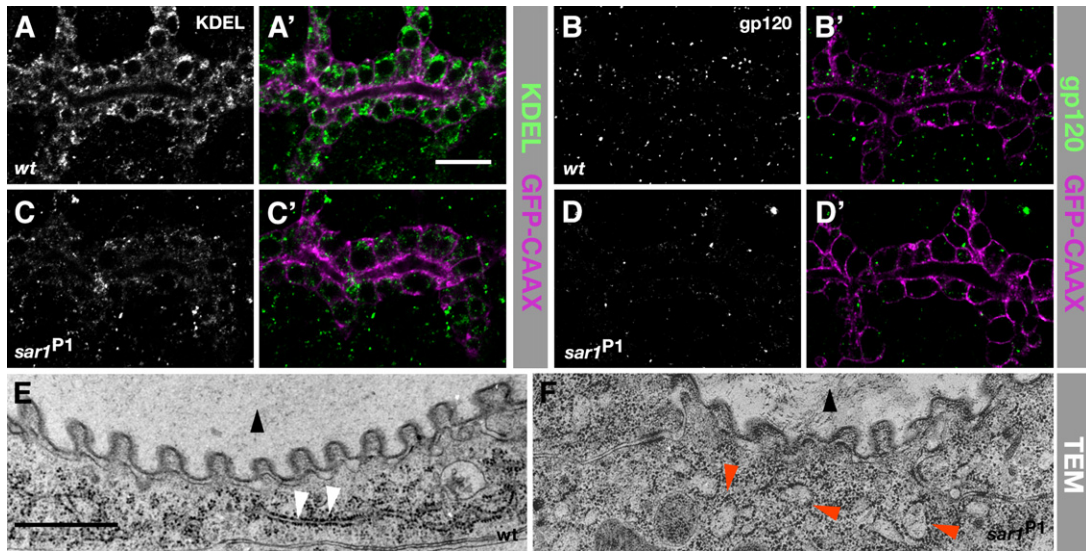


Figure 3. Defective ER and Golgi in *sar1^{P1}* Embryos

(A–D') Confocal sections of stage-14 (A–B') wild-type and (C–D') *sar1^{P1}* mutant embryos expressing *btl* > GFP-CAAX (magenta). Embryos were stained with anti-KDEL for ER (white in [A] and [C] and green in [A'] and [C']) and with anti-gp120 for Golgi (white in [B] and [D] and green in [B'] and [D']). *sar1^{P1}* mutant embryos show a (C and C') disruption of ER and a (D and D') marked decrease of the Golgi staining in the tracheal cells. (E and F) TEM sections of DT of late stage-16 (E) wild-type and (F) *sar1^{P1}* embryos. (E) Wild-type tracheal cells show a tubular organization of the rough ER, tightly lined by dark ribosomes (white arrowheads). (F) In *sar1^{P1}* mutants, tracheal cells show a disrupted and bloated rough ER organization (orange arrowheads). Black arrowheads mark the luminal electron-dense extracellular matrix. (F) Note its distortion in the mutant. Scale bars are 10 μm in (A)–(D') and 1 μm in (E) and (F).

efficient secretion of luminal markers, which are predicted to associate with the growing intraluminal chitin matrix.

Zygotic *sar1* Mutants Have Reduced Sar1 Function in the Trachea

sar1 mRNA has been reported to be abundantly maternally contributed (Zhu et al., 2005). At later stages, zygotic expression of *sar1* mRNA is initiated in multiple epithelial tissues (Abrams and Andrew, 2005). To monitor Sar1 zygotic expression in the trachea, we used a Sar1-GFP protein trap line (Wilhelm et al., 2005). Embryos carrying only paternally derived Sar1-GFP show a strong zygotic expression of GFP in the trachea (Figure S2). We also used an anti-Sar1 antibody to analyze Sar1 expression in the trachea of wild-type, zygotic *sar1^{P1}*, and *sar1^{EP3575Δ28}* null mutant embryos (Zhu et al., 2005) (Figure S2). Both zygotic mutants showed a clear reduction, but not complete elimination, of Sar1 expression in the trachea. To test the effects of a more complete inactivation of Sar1, we generated transgenic flies expressing a dominant-negative *sar1^{T38N}* form in the trachea (Kuge et al., 1994). In *btl* > *sar1^{T38N}*-expressing embryos, we observed early defects in tracheal branching and epithelial integrity as well as a complete block in Verm secretion (Figure S2). In contrast to *btl* > *sar1^{T38N}*-expressing embryos, zygotic *sar1^{P1}* mutant embryos show normal early tracheogenesis with no defects in branching morphogenesis and epithelial integrity (Figure S3).

In summary, tracheal expression of Sar1 is markedly reduced in zygotic *sar1* mutant embryos. While maternally supplied Sar1 is sufficient to support early tracheal devel-

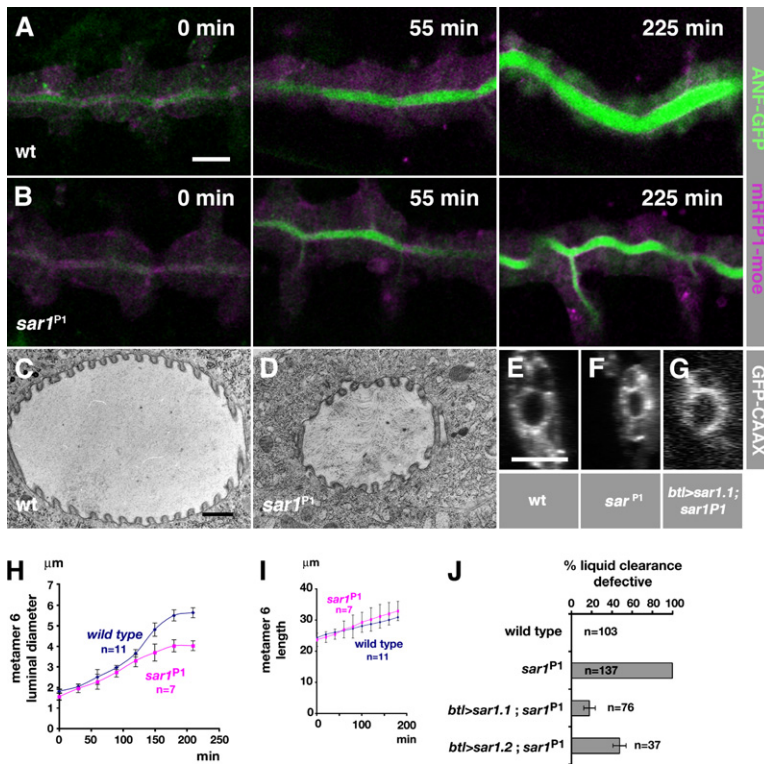
opment, zygotic Sar1 is required for efficient luminal secretion.

Sar1 Localizes to the ER and Is Required for ER and Golgi Integrity

Given the conserved role of Sar1 in vesicle budding from the ER, we determined its subcellular localization in the trachea by using anti-Sar1 antibodies. Sar1 localizes predominantly to the ER (marked by the PDI-GFP trap) (Figure S2). Continuous COPII-mediated transport from the ER is required to maintain the Golgi apparatus and ER structure (Altan-Bonnet et al., 2004; Yamanushi et al., 1996). To test if zygotic loss of Sar1 compromises the integrity of the ER and Golgi in tracheal cells, we stained *sar1* mutant embryos with antibodies against KDEL (marking the ER lumen) and gp120 (highlighting Golgi structures). In *sar1* mutant embryos, we observed a strongly disrupted ER structure and loss of Golgi staining in DT cells at stage 14 (Figures 3A–3D). Additionally, TEM of stage-16 wild-type and *sar1* mutant embryos showed a grossly bloated rough ER structure in DT tracheal cells (Figures 3E and 3F). Consistent with its functions in yeast and vertebrates, *Drosophila* Sar1 localizes to the ER and is not only required for efficient luminal protein secretion, but also for the integrity of the early secretory apparatus.

Zygotic *sar1* Is Selectively Required for Luminal Diameter Expansion

To analyze tracheal maturation defects in *sar1* mutant embryos, we generated and imaged *sar1* strains that carry either *btl* > ANF-GFP *btl*-mRFP-*moe* or *btl* > Gasp-GFP



(Movies S6 and S7). In *sar1* mutants, luminal deposition of both ANF-GFP and Gasp-GFP is reduced (Figures 4A and 4B; Figure S4). Like endogenous Gasp in the mutants, Gasp-GFP was clearly retained in the cytoplasm of *sar1* embryos. ANF-GFP was also retained in the tracheal cells of *sar1* mutants, but to a lesser extent. Strikingly, *sar1* mutants failed to fully expand the luminal diameter of the DT outlined by the apical RFP-moe localization (Figure 4B). We quantified this defect by measuring diametric growth rates in metamere 6 for wild-type (n = 11) and *sar1* mutant (n = 7) embryos. While early lumen expansion commences in parallel in both genotypes, the later diametric growth of *sar1* mutants falls significantly behind compared to wild-type embryos. The DT lumen in *sar1* mutants reaches only an average of 70% (4.05 μm ± 0.2 SEM) of the wild-type diameter (5.75 μm ± 0.2) at early stage 16 (Figure 4H). We detected identical diametric growth defects in fixed *sar1* mutant embryos expressing *btl* > GFP-CAAX by analysis of confocal yz sections or TEM (Figures 4C–4F). Reexpression of *sar1* in the trachea of *sar1* mutant embryos not only rescued secretion, but also the lumen diameter phenotype at stage 16 (Figure 4G). In contrast to the diametric growth defects, DT tube elongation in *sar1* embryos was indistinguishable from that in wild-type (Figure 4I). This demonstrates distinct genetic requirements for tube diameter and length growth. It also reveals that the *sar1* DT luminal volume reaches less than half of the wild-type volume. Prolonged live imaging showed that *sar1* mutants are also completely deficient in luminal protein and liquid clearance (Figure 4J; Figure S4). Up to 80% of the rescued embryos also com-

Figure 4. *sar1* Is Selectively Required for Tube Diameter Expansion

(A and B) Frames from two time-lapse confocal movies showing the luminal secretion burst (0 and 55 min) and diametric expansion (225 min) in (A) wild-type and (B) *sar1*^{P1} embryos expressing *btl* > ANF-GFP (green) and *btl*-mRFP1-*moe* (magenta) (Movie S7). (C and D) TEMs of DT cross-sections from late stage-16 (C) wild-type and (D) *sar1*^{P1} mutant embryos. (E–G) y-z confocal projections of the DT at metamere 6 in late stage-16 (E) wild-type, (F) *sar1*^{P1}, and (G) *btl* > *sar1.1*; *sar1*^{P1} rescued embryos. (H and I) The DT diameter expansion rates at metamere 6 in live embryos. Diameter growth in *sar1*^{P1} mutants is significantly reduced compared to wild-type embryos (p < 0.001). Tube elongation rates in *sar1*^{P1} are indistinguishable from wild-type. Bars are means ± SEM. (J) *sar1*^{P1} embryos are liquid-clearance defective. Transgenic expression of Sar1 specifically in the trachea of *sar1*^{P1} embryos significantly rescued the liquid-clearance phenotype (p < 0.001). Bars are means ± SEM. Scale bars are 10 μm in (A), (B), and (E)–(G) and 1 μm in (C) and (D).

pleted luminal liquid clearance, suggesting that efficient tracheal secretion and the integrity of the secretory apparatus are prerequisites for later tube maturation steps (Figure 4J). Taken together, the above-described results show that tracheal Sar1 is selectively required for tube diameter expansion. Additionally, subsequent luminal protein and liquid clearance fail to occur in *sar1* mutants.

Mutants in COPII Subunits Phenocopy *sar1* Secretion and Diameter Phenotypes

Do the tracheal defects of *sar1* reflect a general requirement for the COPII complex in luminal secretion and diameter expansion? To test this, we analyzed lethal P element insertion alleles disrupting two additional COPII coat subunits, *sec13* and *sec23* (Abrams and Andrew, 2005). We stained mutant *sec13* and *sec23* embryos for luminal Gasp and for Crb and α-Spectrin to highlight tracheal cells. At stage 15, embryos of both mutants show a clear cellular retention of Gasp (Figure S5). Furthermore, stage-16 *sec13* and *sec23* embryos show significantly narrower DT tubes when compared to wild-type. The average diameter of the DT branches in metamere 6 was 4.8 μm (±0.2 μm) and 4.4 μm (±0.1 μm) in fixed *sec13* and *sec23* embryos, respectively, compared to 6.3 μm (±0.1 μm) in wild-type (Figure S5). Therefore, *sec13* and *sec23* mutants phenocopy *sar1*. The phenotypic analysis of three independent mutations disrupting ER-to-Golgi transport thus provides a strong correlation between deficits in luminal protein secretion and tube diameter expansion (Figure 7A).

Luminal Protein Clearance Depends on Tracheal Rab5 Activity and Endocytosis

Anticipating that the wave of luminal protein clearance may depend on endocytic uptake, we screened several mutations with known defects in endocytosis. To directly assess luminal protein clearance, we generated strains of endocytic mutants carrying *btl* > ANF-GFP and analyzed them live. We found that *clathrin heavy chain*¹ (*chc*¹), *shibire*^{ts2} (*shi*^{ts2} at the restrictive temperature of 32°C), and *rab5*² null mutant embryos all display profound defects both in luminal protein and liquid clearance (Figure S6). *Chc* is the heavy chain of the Clathrin coat (Bazinnet et al., 1993), and *shi* codes for the Dynamin GTPase that clips Clathrin-coated pits off the membrane to form endocytic vesicles (van der Bliek and Meyerowitz, 1991). *rab5* encodes for a small GTPase that is a key regulator of early endocytosis (Wucherpfennig et al., 2003). We focused our further analysis on *rab5*, since *rab5*² showed the most penetrant defects in protein clearance (Figure S6). To follow luminal protein clearance live, we imaged wild-type and *rab5*² mutant embryos expressing ANF-GFP or Gasp-GFP. *rab5*² mutant embryos failed to eliminate both luminal GFP markers (Figures 5A–5D; Movies S8–S10). In contrast to wild-type, *rab5*² mutants also retained substantial quantities of endogenous luminal Gasp, Verm, chitin, and 2A12 antigen inside the tracheal tubes (Figures 5E–5H; Figure S6). When we expressed GFP-*rab5* specifically in the trachea of *rab5* mutant embryos, luminal clearance was rescued significantly (Figure 5I). Our analysis thus shows that *rab5* is required in the trachea for proper clearance of luminal proteins and chitin. The additional analysis of *chc*¹ and *shi*^{ts2} mutant embryos argues that not only Rab5, but endocytosis in general, is required for the clearance of luminal solids.

Normal Secretory Capacity and Epithelial Integrity, but Defective Endosomal Structures, in *rab5* Mutants

We examined whether the clearance phenotypes of *rab5* mutants may be secondary to disruptions of either secretion (as for *sar1*) or loss of epithelial integrity. Apart from a minor and partially penetrant tube elongation phenotype, *rab5*² mutants develop an essentially wild-type tracheal network. They show normal secretion of luminal markers at stage 15, as well as intact tracheal epithelial polarity at stage 16. We also analyzed DTs of late stage-16 *rab5*² mutant embryos by TEM. These embryos display a wild-type cellular ultrastructure and apical luminal lining in the DT tubes (Figure S7). Finally, we performed a dextran injection assay that showed that *rab5*² mutant embryos have intact paracellular junctions (Figure S9). Thus, zygotic *rab5* mutant embryos show an overall normal tracheal development and secretion.

We tested the integrity of several distinct endosomal compartments in *rab5*² mutants. We visualized Clathrin-coated vesicles (CCV) by using anti-*Chc* antibodies in fixed embryos. We also used GFP-tagged reporters expressed in the trachea to analyze early endosomes (EE) and multivesicular bodies (MVB) by using GFP-myc-

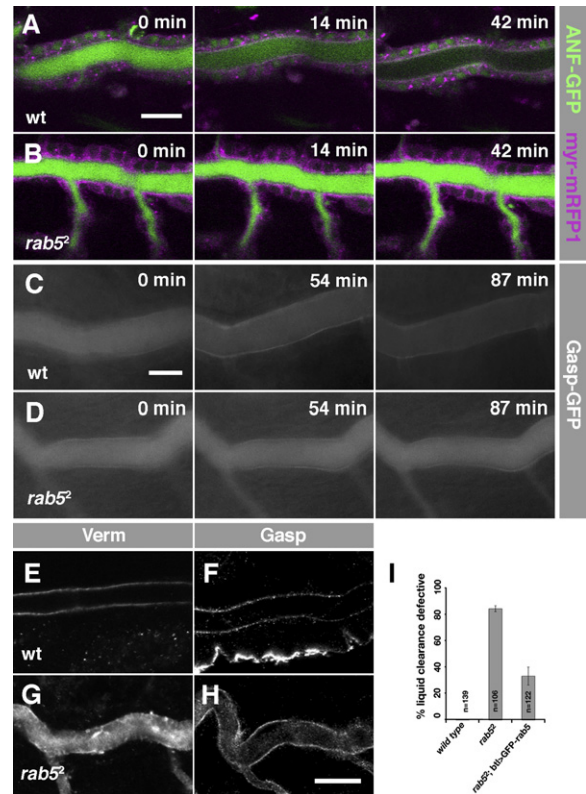


Figure 5. Luminal Protein Clearance Requires Rab5-Mediated Endocytosis

(A and B) Selected frames from a time-lapse confocal movie showing the clearance of ANF-GFP (green) in a live (A) wild-type and a (B) *rab5*² embryo. DT tracheal cells were marked by *btl* > myr-mRFP1 (magenta). Wild-type embryos clear ANF-GFP from the lumen while *rab5*² embryos retain it (Movie S8).

(C and D) Wide-field images from a time-lapse movie of a (C) wild-type and a (D) *rab5*² mutant embryo expressing Gasp tagged with GFP (*btl* > Gasp-GFP) (Movies S9 and S10). *rab5*² embryos retain Gasp-GFP inside the lumen.

(E–H) Confocal sections of DT in late stage-17 (E and F) wild-type and (G and H) *rab5*² mutant embryos stained with (E and G) Verm and (F and H) Gasp (white). *rab5*² mutant embryos retain endogenous luminal antigens at late stage 17.

(I) Plot showing the percentage of liquid-clearance defects in wild-type, *rab5*², and *rab5*²; *btl* > GFP-*rab5* embryos. There is a significant reduction of defects in *rab5*²; *btl* > GFP-*rab5* (rescue embryos) compared to *rab5*² embryos ($p < 0.001$, two-tailed t test). Bars represent means \pm SEM.

Scale bars are 10 μ m.

2x-FYVE, recycling endosomes (RE) by using GFP-Rab11, and late endosomes (LE) by using GFP-Rab7 (Emery et al., 2005; Wucherpfennig et al., 2003). For the latter three markers, the analysis of live and fixed embryos yielded identical results.

We found no changes between wild-type and *rab5*² mutant embryos in the predominantly apical localization of GFP-Rab11-positive REs (Figure S8). The remaining endocytic markers were also unaffected during tracheal development in *rab5*² mutant embryos up to early stage

17. However, at mid-stage 17, during the period of luminal protein clearance, the cellular distribution of Chc, GFP-FYVE, and GFP-Rab7 was clearly aberrant in *rab5*² mutant embryos.

In wild-type mid-stage-17 embryos, the majority of Chc was localized apically in a discrete, dotted pattern. In the DT of *rab5*² mutants, this discrete localization of Chc was lost (Figure S8). Live imaging of *btl* > GFP-FYVE embryos at mid-stage 17 reveals the dynamic movement of large, GFP-FYVE-positive apical structures in the tracheal cells in a background of small endosomal vesicles. Strikingly, GFP-FYVE labeling of those apical structures was absent in *rab5*² mutants, leaving few, small and randomly distributed vesicles (Figure S8; Movie S11). The lack of the extensive GFP-FYVE-positive structures in the mutants may either reflect the function of Rab5 generating the FYVE ligand phosphatidylinositol-3-phosphate or a direct role of Rab5 in endosomal assembly and growth (Christoforidis et al., 1999). In wild-type, GFP-Rab7 highlights late endosomal structures spread along the apicobasal axis of the tracheal cells. In most *rab5* mutant embryos, the abundance of GFP-Rab7 endosomes was decreased or completely lost (Figure S8).

Taken together, *rab5* mutants show normal epithelial development and secretion in the trachea, but aberrant localization and abundance of Chc-, GFP-FYVE-, and GFP-Rab7-positive structures at mid-stage 17. This suggests that Rab5 either directly mediates or indirectly facilitates the formation and intracellular organization of CCVs and LEs. The manifestation of endocytic phenotypes in the trachea of *rab5*² mutants precisely correlates with the initiation of solid luminal material clearance in the wild-type.

The Tracheal Epithelium Directly Internalizes and Clears Luminal Material by Endocytosis

Our mutant analysis shows that endocytosis is required for luminal material clearance. Protein trafficking through endocytic compartments may either directly absorb and clear luminal proteins or indirectly facilitate the extinction of luminal material. If the tracheal epithelium directly internalizes luminal material by endocytosis, we expect that: (1) tracheal cells take up luminal markers, and that (2) luminal markers colocalize with endosomal structures inside the tracheal cells during tube clearance.

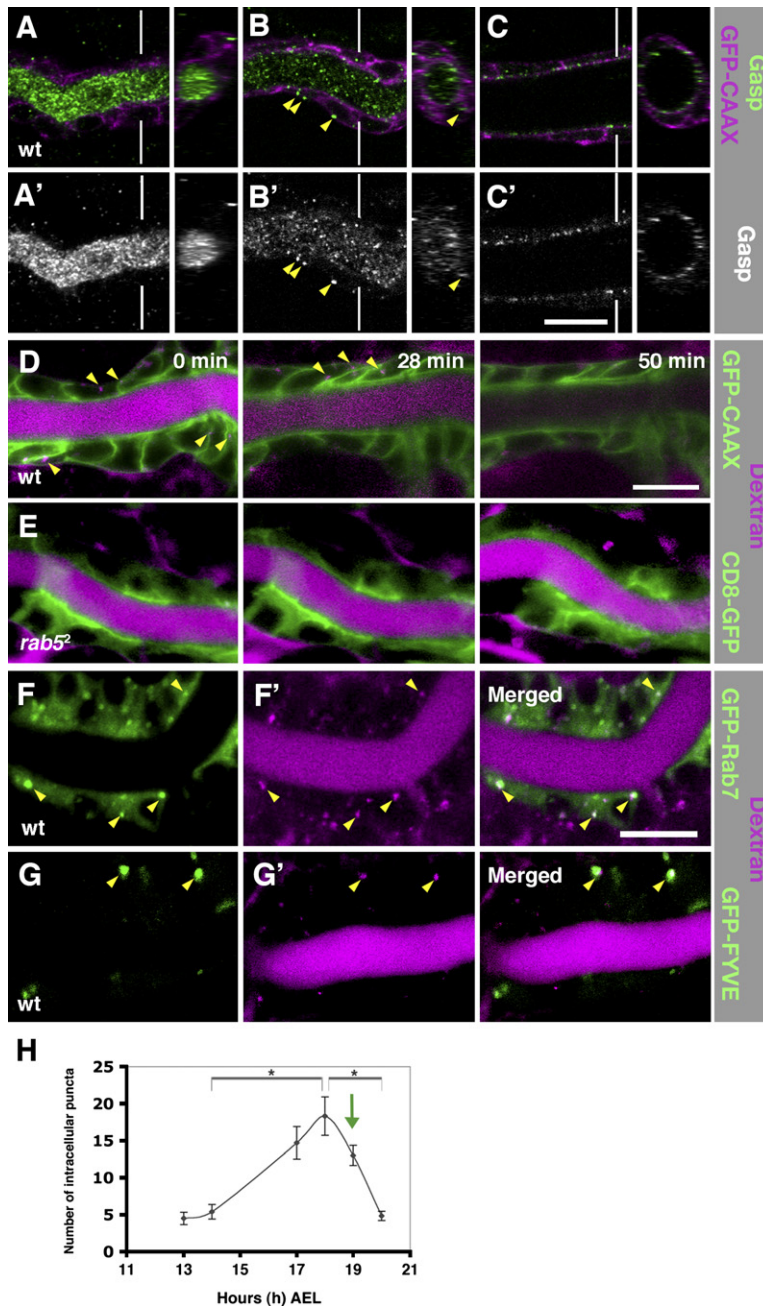
To test if endogenous proteins are taken up into tracheal cells during luminal solid clearance, we used an amplified staining protocol that allows for the detection of the luminal marker Gasp in mid-stage-17 embryos. *gasp* mutants were devoid of any Gasp staining throughout tracheal development (Figure S9; K.T. and C.S., in preparation). In early stage-16 embryos marked by *btl* > GFP-CAAX, Gasp localized almost completely inside the lumen of the DT (Figure 6A). From early to mid-stage 17, a large number of intracellular Gasp puncta became apparent in the tracheal cells (Figure 6B; Figure S9). At late stage 17, the remaining Gasp was mainly localized along the apical tube lining (Figure 6C). Thus, intracellular Gasp levels transiently increase before and during the period of luminal protein clearance.

We analyzed the distribution of intracellular Gasp puncta relative to endosomal markers in the trachea of fixed embryos. We tested the following genotypes of embryos for colocalization: *btl* > Clathrin light chain-GFP (Clc-GFP) for CCVs, *btl* > GFP-Rab5 for EEs, *btl* > GFP-Rab7 for LEs, and *btl* > GFP-LAMP1 (GFP-Lysosomal Associated Membrane Protein 1) for lysosomes (Chang et al., 2002; Pulipparacharuvil et al., 2005). While intracellular Gasp staining only occasionally colocalized with GFP-Rab5-positive endosomes, Gasp puncta more consistently colocalized with Clc-GFP, GFP-Rab7, and GFP-LAMP1 staining (Figure S9). Thus, considerable portions of intracellular Gasp staining coincide with CCVs, LEs, and lysosomal markers, suggesting that Gasp may traverse those endosomal compartments. The lysosomal localization of intracellular Gasp indicates that Gasp may be degraded inside tracheal cells during clearance of solid luminal material.

While the detection of endogenous Gasp in endosomal structures during stage 17 argues for a direct role of endocytosis in tube clearance, the localization of intracellular Gasp puncta to specific endosomal compartments was relatively infrequent. To visualize the cellular dynamics during luminal protein clearance directly, we established a live endocytosis assay in the trachea by using the fluid-phase marker dextran (Swanson, 1989). We injected 10 kDa dextran into the hemocoel of stage-13 to stage-14 embryos, which lack the paracellular barrier function provided by fully assembled septate junctions (Tepass and Hartenstein, 1994). In these experiments, the fluorescent dextran consistently accumulated inside the tracheal lumen of wild-type embryos (Figure 6D). Taking advantage of this assay, we preloaded the trachea of *btl* > ANF-GFP embryos with rhodamine-labeled dextran and live imaged ANF-GFP along with the injected marker. Both ANF-GFP and dextran were cleared from the DT lumen simultaneously (Movie S12), suggesting that exogenous luminal dextran is cleared similarly to other luminal constituents.

Is dextran taken up into tracheal cells during luminal protein clearance? We injected 10 kDa dextran into early embryos carrying the tracheal *btl* > GFP-CAAX marker and analyzed them. We initially detected only few intracellular puncta in such embryos at stage 16 (Figure 6H and data not shown). However, from early to mid-stage 17 and before the drop in luminal fluorescent intensity, the number of rhodamine-dextran puncta distinctly increased inside tracheal cells (Figure 6D, 0 min and 28 min). Upon luminal clearance completion (late stage 17), the count of intracellular dextran puncta was diminished to basal levels (Figure 6D, 50 min). Quantification of intracellular dextran puncta demonstrates a dynamic peak of dextran internalization just before and during luminal protein clearance (Figure 6H).

Since not all of the injected dextran is taken up into the tracheal lumen, the detected intracellular dextran signals may derive either from the lumen or the hemocoel. To test the origin of intracellular dextran, we injected rhodamine-labeled dextran into the hemocoel of late stage-16 embryos. These embryos display fully developed



paracellular barriers that prevent the luminal access of the 10 kDa dextran (Lamb et al., 1998). Importantly, we did not find any fluorescent signal inside the tracheal cells at mid-stage 17 in such embryos (Figure S9). This demonstrates that the transient intracellular dextran puncta in embryos preloaded at stage 13 indeed derive from the lumen. We next asked if dextran internalization requires Rab5-dependent endocytosis. We injected rhodamine-labeled dextran into *rab5²* mutant embryos with tracheal cells labeled by *btl* > CD8-GFP. A total of 56% of *rab5²* mutant embryos ($n = 11$) failed to show the characteristic transient peak of intracellular dextran accumulation during the period of

luminal protein clearance (Figure 6E). Thus, tracheal cells internalize the preloaded dextran from the lumen in a Rab5-dependent manner exactly before and during the peak of luminal solid clearance.

To test if intracellular dextran dots localize to endosomes, we expressed GFP-Rab5, GFP-2x-FYVE, and GFP-Rab7 in the trachea under the control of *btl*-GAL4. Embryos of each genotype were preloaded with 10 kDa rhodamine-labeled dextran and analyzed live during its luminal clearance. While localization of dextran to GFP-Rab5-marked EEs was very rare (data not shown, 1.3%, $n = 8$ embryos), the proportion of dextran puncta localizing

Figure 6. Trachea Cells Directly Remove Luminal Material through Endocytosis

(A–C) (A–C) Confocal xy sections and yz projections of DT of wild-type embryos expressing *btl* > GFP-CAAX at (A) stage 16, (B) mid-stage 17, and (C) late stage 17. yz confocal sections correspond to the DT position indicated by thin, vertical lines in xy sections. Embryos were stained with anti-Gasp (green) and anti-GFP (magenta). (A'–C') Gasp staining (white) of the images in (A), (B), and (C). The number of intracellular Gasp puncta (arrowheads) increases during the period of luminal protein clearance at mid-stage 17 and decreases afterwards.

(D and E) Frames from a time-lapse confocal analysis before (0 min), during (28 min), and after (50 min) protein clearance of a dextran-preloaded (D) wild-type and a (E) *rab5²* live embryo expressing *btl* > GFP-CAAX and *btl* > GFP-CD8, respectively. Intracellular puncta of luminal dextran are present just before (0 min) and during (28 min) luminal protein clearance in wild-type (arrowheads), but not in *rab5²* mutant, embryos. Luminal dextran clearance is defective in *rab5²* embryos ($n = 11$).

(F–G') Images from confocal time-lapse analysis of dextran-injected embryos expressing the endosomal markers (F) *btl* > GFP-Rab7 and (G) *btl* > GFP-FYVE, just before protein clearance. A proportion of intracellular dextran puncta localize to GFP-Rab7- or GFP-FYVE-positive endosomes (arrowheads).

(H) The dynamics of endocytosed tracheal puncta during late embryonic development. A significant increase in the number of internalized dextran occurs before luminal protein clearance (17–19 hr AEL). The green arrow indicates the time of luminal clearance. Values represent mean and standard error from five independent experiments. For all developmental time points $n = 24$, except for 13 hr AEL, where $n = 8$. The asterisk denotes $p < 0.01$ by Student's *t* test comparing the data sets between two time points. Bars represent means \pm SEM. Scale bars are 10 μ m.

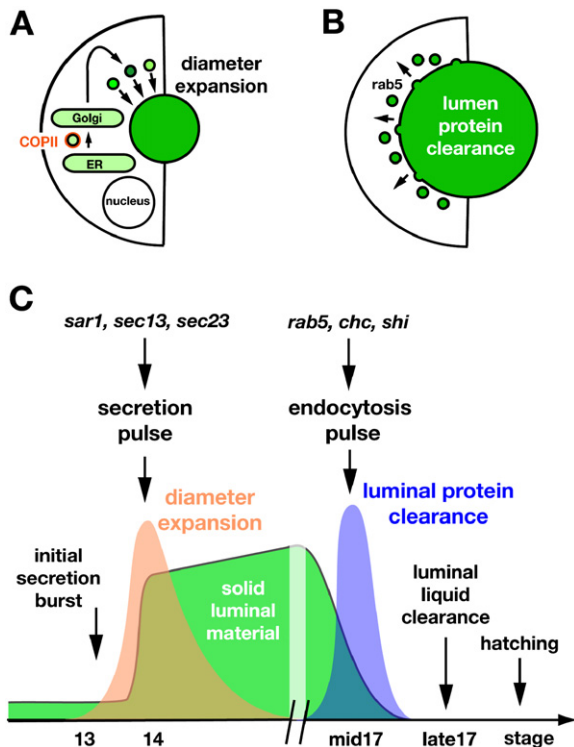


Figure 7. Distinct Pulses of Secretion and Endocytosis Drive Tracheal Airway Maturation

(A and B) Schematic illustration of a cross-section through a DT at (A) stage 14 and at (B) early stage 17. (A) The ER, Golgi, and post-Golgi vesicles carry luminal proteins (green) into the lumen. COPII vesicular transport from the ER to the Golgi is required for efficient luminal secretion and diameter expansion. (B) After diametric expansion, tracheal cells internalize and clear luminal content (green) by Rab5-dependent endocytosis.

(C) Schematic model of airway maturation based on live-imaging and mutant analysis. The solid luminal content is indicated in green. The initial secretion burst extends into a massive, continued secretion pulse (orange) of chitin-binding proteins that fill the lumen. The COPII-dependent secretion pulse is essential for luminal matrix assembly and tube diameter expansion. At early stage 17, the tracheal epithelium activates a pulse of endocytic activity (blue) that internalizes and removes solid contents from the lumen. The endocytosis pulse requires the function of Rab5, Clathrin, and Dynamin. The two pulses represent peaks of cellular activity above the background of basal cellular secretion and endocytosis, which, for simplicity, are not shown in the model.

to GFP-FYVE-positive EE and MVBs, and to GFP-Rab7-marked LEs, was 8.0% and 31%, respectively ($n = 5$) (Figure 6F).

In summary, our data show that endogenous Gasp and injected rhodamine-labeled dextran are internalized by tracheal cells before and during the clearance interval. Both markers localize to endosomal structures in tracheal cells (Figure 7B). We conclude that the tracheal epithelium directly removes luminal Gasp protein and the preloaded dextran polymers by a transient, Rab5-dependent, endocytic wave.

DISCUSSION

Our live-imaging approach defines the developmental dynamics of functional tracheal maturation. At the organ level, we identified three sequential and rapid developmental transitions: (1) the secretion burst, followed by massive luminal protein deposition and tube diameter expansion, (2) the clearance of solid luminal material, and (3) the replacement of luminal liquid by gas. Live imaging of each event additionally revealed insights into the startlingly dynamic activities of the tracheal cells. ANF-GFP-containing structures and apical GFP-FYVE-positive endosomes rapidly traffic in tracheal cells during the secretion burst and protein clearance. The direct live comparison between wild-type and mutant embryos further highlights the dynamic nature of epithelial activity during each pulse.

We identified several mutations that selectively disrupt distinct cellular functions and concurrently interrupt the maturation process at specific steps. This clearly demonstrates the significance of phenotypic transitions in epithelial organ maturation and establishes that secretion is required for luminal diameter expansion and endocytosis for solid luminal material clearance.

The Secretory Burst and Tube Diameter Expansion

The sudden initiation of an apical secretory burst tightly precedes diametric tube expansion. The completion of both events depends on components of the COPII complex, further suggesting that the massive luminal secretion is functionally linked to diametric growth. How does apical secretion provide a driving force in tube diameter expansion? In mammalian lung development, the distending internal pressure of the luminal liquid on the epithelium expands the lung volume and stimulates growth. Cl^- channels in the epithelium actively transport Cl^- ions into luminal liquid. The resulting osmotic differential then forces water to enter the lung lumen, driving its expansion (Olver et al., 2004). By analogy, the tracheal apical exocytic burst may insert protein regulators such as ion channels into the apical cell membrane or add additional membrane to the growing luminal surface. Since the ER is a crucial cellular compartment for intracellular traffic and lipogenesis, its disruption in *sar1* mutants may disrupt the efficient transport of so far unknown specific regulators or essential apical membrane addition required for diametric expansion. Alternatively, secreted chitin-binding proteins (ChB) may direct an increase of intraluminal pressure and tube dilation. Overexpression of the chitin-binding proteins Serp-GFP or Gasp-GFP was insufficient to alter the diametric growth rate of the tubes, suggesting that lumen diameter expansion is insensitive to increased amounts of any of the known luminal proteins (unpublished data). In *sar1* mutants, the secretion of at least two chitin-binding proteins, Gasp and Verm, is reduced. Chitin, however, is deposited in seemingly normal quantities, but assembles into an aberrantly narrow and dense chitinous cable. This phenotype suggests that the correct ratio between chitin and multiple interacting proteins may be required

for the correct assembly of the luminal cable. Interestingly, *sar1*, *sec13*, and *sec23* mutant embryos form a severely defective and weak epidermal cuticle (Abrams and Andrew, 2005). The luminal deposition of ChB proteins during the tracheal secretory burst may orchestrate the construction and swelling of a functional matrix, which, in turn, induces lumen diameter dilation. While we favor this later hypothesis, we cannot exclude that other mechanisms, either separately or in combination with the dilating luminal cable, drive luminal expansion (Figure 7A).

Endocytotic Clearance of Luminal Material

During tube expansion, massive amounts of luminal material, including the chitinous cable, fill the tracheal tubes. We found that Dynamin, Clathrin, and the tracheal function of Rab5 are required to rapidly remove luminal contents, indicating that endocytosis is required for this process. Several lines of evidence argue that the tracheal epithelium activates Rab5-dependent endocytosis to directly internalize luminal material. First, the tracheal cells of *rab5* mutants show defects in multiple endocytic compartments. These phenotypes of *rab5* mutants become apparent during the developmental period matching the interval of luminal material clearance in wild-type embryos. Second, tracheal cells internalize two luminal markers, the endogenously encoded Gasp and the dextran reporter, exactly prior and during luminal protein clearance. The number of intracellular dextran puncta reaches its peak during the clearance process and ceases shortly thereafter. Lastly, intracellular puncta of both Gasp and dextran colocalize with defined endocytic markers inside tracheal cells. The colocalization of Gasp and dextran with GFP-Rab7 and of Gasp with GFP-LAMP1 suggests that the luminal material may be degraded inside tracheal cells. Taken together, our data show that the tracheal epithelium activates a massive wave of endocytosis to clear the tubes (Figure 7B).

Endocytic routes are defined by the nature of the internalized cargoes and the engaged endocytic compartments (Conner and Schmid, 2003). What may be the features of the endocytic mechanisms mediating the clearance of luminal material? The phenotype of *chc* mutants and the presence of intracellular Gasp in CCVs indicate that luminal clearance at least partly relies on Clathrin-mediated endocytosis (CME). In addition to CME, Dynamin and Rab5 have also been implicated in other routes of endocytosis, suggesting that multiple endocytic mechanisms may be operational in tracheal maturation. The nature of the endocytosed luminal material provides an additional perspective. While cognate uptake receptors may exist for specific cargoes such as Gasp, Verm, and Serp, the heterologous ANF-GFP, degraded chitin, and the fluid-phase marker dextran may be cleared by either fluid-phase internalization or multifunctional scavenger receptors. Interestingly, Rab5 can regulate fluid-phase internalization in cultured cells by stimulating macro-pinocytosis and the activation of Rabankyrin-5 (Bucci et al., 1992; Schnatwinkel et al., 2004; Stenmark et al., 1994). The defective tracheal internalization of

dextran in *rab5* mutants provides further loss-of-function evidence for Rab5 function in fluid-phase endocytosis in vivo. The above-described arguments lead us to speculate that additional Rab5-regulated endocytic mechanisms most likely cooperate with CME in the clearance of solid luminal material.

How is liquid cleared from the lumen? While we still know very little about this fascinating process (Kallis, 1939), some developmental and mechanistic arguments suggest that this last maturation step is mechanistically distinct. First, the interval of luminal liquid clearance is clearly distinct from the period of endocytic clearance of solids. Second, the dynamic internalization of dextran and the abundance of GFP-marked endocytic structures decline before liquid clearance. Finally, our assessment of liquid clearance further suggests that it requires a distinct cellular mechanism (K.-A.S. and V.T., unpublished data).

Viewing the entire process of airway maturation in conjunction, some general conclusions may be drawn. First, the three epithelial pulses are highly defined by their sequence and exact timing, suggesting that they may be triggered by intrinsic or external cues. Second, the analysis of mutants that selectively reduce the amplitude of the secretory or endocytic pulses demonstrates the requirement for each epithelial transition in the completion of the entire maturation process. These pulses are induced in the background of basal secretory and endocytic activities that operate throughout development. Third, specific cellular activities exactly precede each morphological transition. Finally, the separate transitions are interdependent in a sequential manner. Efficient secretion is a prerequisite for the endocytic wave. Similarly, protein endocytosis is a condition for luminal liquid clearance. This suggests a hierarchical coupling of the initiation of each pulse to completion of the previous one in a strict developmental sequence (Figure 7C).

Our study provides a striking example of how pulses of epithelial activity drive distinct developmental events and mold the nascent tracheal lumen into an air delivery tube. Our findings are likely to be relevant beyond the scope of tracheal development. The uniform growth of salivary gland tubes in flies and the excretory canal and amphid channel lumen in worms also require the assembly of a luminal matrix for uniform tube growth (Abrams et al., 2006; Perens and Shaham, 2005). Luminal material is also transiently present during early developmental stages in the distal nephric ducts of lamprey (Youson, 1984). Thus, the coordinated, timely deposition and removal of transient luminal matrices may represent a general mechanism in tubulogenesis.

EXPERIMENTAL PROCEDURES

Genetics

The P element alleles */(3)s009124* (*sar1^{P1}* in text) and */(3)05712* fail to complement the nulls *sar1^{EP3575Δ28, Δ71}* and the GFP trap *sar1^{CA07674}*. Insertion sites were determined by plasmid rescue and PCR. Precise excision of *sar1^{P1}* reverted tracheal phenotypes. The COPII subunit

mutations are *l(3)01031 (sec13)* and *l(3)j13C8 (sec23)*. For more strain information, see the [Supplemental Data](#).

Molecular Biology

PCR subcloning was used to generate pET28a His-Gasp (14–189 aa) for recombinant protein expression and pUAST-Gasp-GFP construction from clones RH12464 and RH10284, respectively. Purified recombinant Gasp was used to immunize guinea pigs. pUAST-*sar1* and pUAST-*sar1*^{T38N} were generated by subcloning of RE74312 and PCR mutagenesis.

Immunostaining, TEM, and Dextran Injections

Immunohistochemistry, TEM and 10 kDa dextran (Molecular Probes) injections was performed as described (Lamb et al., 1998; Wang et al., 2006). Additional antibodies used were: guinea pig anti-Coracle (from R.G. Fehon), mouse mAb anti-gp120/Golgi (clone7H6D7C2, Calbiochem), mouse mAb anti-KDEL (clone10C3, Nordic Biosite), goat anti-Clathrin (Sigma), chicken anti-Human Sar1 (Uprosoci Inc.), and guinea pig anti-Gasp. DmSar1 protein is 70% identical to HsSar1. Anti-Gasp staining was amplified using a secondary goat anti-guinea pig and tertiary donkey anti-goat antibodies.

Live Imaging

For wide-field live imaging, dechorionated embryos were mounted on a gas-permeable membrane stretched over two silicon bars on the top of a slide. Embryos were imaged on an Axioplan2 microscope by using either a x20/0.5NA Plan-Neofluar or a x63/1.3NA C-Apochromat water-immersion objective and an attached CCD camera controlled by the AxioVision software 4.5. Generally, 12–17 focal sections (0.5–2.5 μm apart) were recorded every 1–3 min. For confocal live imaging, a laser-scanning confocal microscope (LSM 510 META, Zeiss) with an Argon 2/488 nm, a HeNe 543 nm laser, and a 63/1.3NA C-Apochromat water-immersion objective was used. Individual Z stacks with a step size of 0.7–1.0 μm were taken every 2–4 min over a 2–5 hr period. Time-lapse movies were created from the Z stacks by using NIH ImageJ (Abramoff et al., 2004); <http://rsb.info.nih.gov/ij/>. Live imaging was typically conducted for tracheal metameres 6–8.

ANF-GFP Localization Dynamics and DT Morphometric Analysis

btl > ANF-GFP embryos were collected for 10 min, dechorionated, and imaged by wide-field microscopy. ANF-GFP localization was scored every 5 min for a period of at least 3 hr. The analysis covered 1 or 2 maturation events for 237 embryos at 25°C.

The secretory pulse initiates at 10 hr 30 min (± 17 min, $n = 45$) and is followed by diameter expansion starting at 11 hr 03 min (± 16 min, $n = 24$). ANF-GFP is removed at 18 hr 48 min (± 22 min, $n = 58$), and luminal liquid clearance occurs at 20 hr 8 min (± 18 min, $n = 56$). The embryo hatches at 21 hr 29 min (± 29 min, $n = 108$). We also recorded developing *btl* > ANF-GFP embryos at 22°C during the entire maturation process ($n = 7$). This analysis showed the same order of events with the following time profile: luminal secretion at 12 hr 6 min (± 18 min), diameter expansion at 13 hr 18 min (± 14 min), protein clearance at 21 hr 50 min (± 21 min), and liquid clearance at 24 hr 10 min (± 20 min).

The diameter and length of DT6 were measured in live embryos expressing ANF-GFP and *btl*-mRFP1-*moe*. The diameter was measured at a right angle in three separate positions within metamere 6 for each sample to average tube tapering. Tube length was measured by tracing the apical mRFP1-*moe* from fusion cells DTa6 to DTP6. Recordings covered a period of 4.5 hr with 5 min elapsed time. All measurements were done with AxioVision 4.5 (Zeiss).

Phenotypic Analysis of Endocytic Compartments in Live Embryos

The diameter of endosomal compartments labeled by GFP-FYVE was measured from Z stacks of ten tracheal cells per embryo labeled by *btl* > myr-mRFP1. Endosomal structures with a diameter < 3 μm were not included in the assessment. The number of positive GFP-Rab7 structures was estimated from wide-field sections. Five to six time

points, 15 s apart, were estimated for each embryo. The measurements were assembled with AxioVision 4.5. Intracellular puncta of dextran were assessed from Z stacks of confocal sections (DT metamere 7).

Supplemental Data

Supplemental Data include 12 movies, 9 figures, Supplemental Experimental Procedures, and Supplemental References and are available at <http://www.developmentalcell.com/cgi/content/full/13/2/214/DC1/>.

ACKNOWLEDGMENTS

We would like to thank David L. Deitcher, Marcos González-Gaitán, Markus Affolter, Maria Leptin, Rick Fehon, Alain Debec, Jürgen Knoblich, Helmut Krämer, Allan Spradling, Greg Beitel, the Bloomington Drosophila Stock Center, the Drosophila Genomics Resource Center (DGRC; Indiana), and the Developmental Studies Hybridoma Bank (DSHB; Iowa) for fly strains, clones, and antibodies. We would like to thank Monika Björk and Inger Granell for expert technical assistance. We are grateful to members of the Samakovlis lab, Harald Stenmark, Elisabeth Knust, and Gabriele Senti for discussions and critical comments on the manuscript. K.-A.S. acknowledges a European Molecular Biology Organization long-term fellowship. This work was funded by grants of National Research Council (VR), SSF, and WCN to C.S.

Received: April 23, 2007

Revised: June 15, 2007

Accepted: June 18, 2007

Published: August 6, 2007

REFERENCES

- Abramoff, M.D., Magelhaes, P.J., and Ram, S.J. (2004). Image processing with ImageJ. *Biophotonics International* 11, 36–42.
- Abrams, E.W., and Andrew, D.J. (2005). CrebA regulates secretory activity in the *Drosophila* salivary gland and epidermis. *Development* 132, 2743–2758.
- Abrams, E.W., Mihoulides, W.K., and Andrew, D.J. (2006). Fork head and Sage maintain a uniform and patent salivary gland lumen through regulation of two downstream target genes, *PH4 α SG1* and *PH4 α SG2*. *Development* 133, 3517–3527.
- Affolter, M., Bellusci, S., Itoh, N., Shilo, B., Thiery, J.P., and Werb, Z. (2003). Tube or not tube: remodeling epithelial tissues by branching morphogenesis. *Dev. Cell* 4, 11–18.
- Altan-Bonnet, N., Sougrat, R., and Lippincott-Schwartz, J. (2004). Molecular basis for Golgi maintenance and biogenesis. *Curr. Opin. Cell Biol.* 16, 364–372.
- Barry, M.K., Triplett, A.A., and Christensen, A.C. (1999). A peritrophin-like protein expressed in the embryonic tracheae of *Drosophila melanogaster*. *Insect Biochem. Mol. Biol.* 29, 319–327.
- Bazinet, C., Katzen, A.L., Morgan, M., Mahowald, A.P., and Lemmon, S.K. (1993). The *Drosophila* clathrin heavy chain gene: clathrin function is essential in a multicellular organism. *Genetics* 134, 1119–1134.
- Bonifacino, J.S., and Glick, B.S. (2004). The mechanisms of vesicle budding and fusion. *Cell* 116, 153–166.
- Bucci, C., Parton, R.G., Mather, I.H., Stunnenberg, H., Simons, K., Hoflack, B., and Zerial, M. (1992). The small GTPase rab5 functions as a regulatory factor in the early endocytic pathway. *Cell* 70, 715–728.
- Chang, H.C., Newmyer, S.L., Hull, M.J., Ebersold, M., Schmid, S.L., and Mellman, I. (2002). Hsc70 is required for endocytosis and clathrin function in *Drosophila*. *J. Cell Biol.* 159, 477–487.
- Christoforidis, S., Miaczynska, M., Ashman, K., Wilm, M., Zhao, L., Yip, S.C., Waterfield, M.D., Backer, J.M., and Zerial, M. (1999). Phosphatidylinositol-3-OH kinases are Rab5 effectors. *Nat. Cell Biol.* 1, 249–252.
- Conner, S.D., and Schmid, S.L. (2003). Regulated portals of entry into the cell. *Nature* 422, 37–44.

- Devine, W.P., Lubarsky, B., Shaw, K., Luschnig, S., Messina, L., and Krasnow, M.A. (2005). Requirement for chitin biosynthesis in epithelial tube morphogenesis. *Proc. Natl. Acad. Sci. USA* *102*, 17014–17019.
- Emery, G., Hutterer, A., Berdnik, D., Mayer, B., Wirtz-Peitz, F., Gaitan, M.G., and Knoblich, J.A. (2005). Asymmetric Rab 11 endosomes regulate delta recycling and specify cell fate in the *Drosophila* nervous system. *Cell* *122*, 763–773.
- Ghabrial, A., Luschnig, S., Metzstein, M.M., and Krasnow, M.A. (2003). Branching morphogenesis of the *Drosophila* tracheal system. *Annu. Rev. Cell Dev. Biol.* *19*, 623–647.
- Hogan, B.L., and Kolodziej, P.A. (2002). Organogenesis: molecular mechanisms of tubulogenesis. *Nat. Rev. Genet.* *3*, 513–523.
- Jazwinska, A., Ribeiro, C., and Affolter, M. (2003). Epithelial tube morphogenesis during *Drosophila* tracheal development requires Piopio, a luminal ZP protein. *Nat. Cell Biol.* *5*, 895–901.
- Kallis, N. (1939). The effect on development of a lethal deficiency in *Drosophila melano*: with a description of the normal embryo at hatching. *Genetics* *24*, 244–270.
- Kamei, M., Saunders, W.B., Bayless, K.J., Dye, L., Davis, G.E., and Weinstein, B.M. (2006). Endothelial tubes assemble from intracellular vacuoles in vivo. *Nature* *442*, 453–456.
- Kuge, O., Dascher, C., Orci, L., Rowe, T., Amherdt, M., Plutner, H., Ravazzola, M., Tanigawa, G., Rothman, J.E., and Balch, W.E. (1994). Sar1 promotes vesicle budding from the endoplasmic reticulum but not Golgi compartments. *J. Cell Biol.* *125*, 51–65.
- Lamb, R.S., Ward, R.E., Schweizer, L., and Fehon, R.G. (1998). *Drosophila* coracle, a member of the protein 4.1 superfamily, has essential structural functions in the septate junctions and developmental functions in embryonic and adult epithelial cells. *Mol. Biol. Cell* *9*, 3505–3519.
- Lubarsky, B., and Krasnow, M.A. (2003). Tube morphogenesis: making and shaping biological tubes. *Cell* *112*, 19–28.
- Luschnig, S., Batz, T., Armbruster, K., and Krasnow, M.A. (2006). *serpentine* and *vermiform* encode matrix proteins with chitin binding and deacetylation domains that limit tracheal tube length in *Drosophila*. *Curr. Biol.* *16*, 186–194.
- Martin-Belmonte, F., Gassama, A., Datta, A., Yu, W., Rescher, U., Gerke, V., and Mostov, K. (2007). PTEN-mediated apical segregation of phosphoinositides controls epithelial morphogenesis through Cdc42. *Cell* *128*, 383–397.
- Myat, M.M., and Andrew, D.J. (2002). Epithelial tube morphology is determined by the polarized growth and delivery of apical membrane. *Cell* *111*, 879–891.
- Olver, R.E., Walters, D.V., and M. Wilson, S. (2004). Developmental regulation of lung liquid transport. *Annu. Rev. Physiol.* *66*, 77–101.
- Perens, E.A., and Shaham, S. (2005). *C. elegans* *daf-6* encodes a patched-related protein required for lumen formation. *Dev. Cell* *8*, 893–906.
- Pulipparacharuvil, S., Akbar, M.A., Ray, S., Sevrioukov, E.A., Haberman, A.S., Rohrer, J., and Kramer, H. (2005). *Drosophila* Vps16A is required for trafficking to lysosomes and biogenesis of pigment granules. *J. Cell Sci.* *118*, 3663–3673.
- Rao, S., Lang, C., Levitan, E.S., and Deitcher, D.L. (2001). Visualization of neuropeptide expression, transport, and exocytosis in *Drosophila melanogaster*. *J. Neurobiol.* *49*, 159–172.
- Ribeiro, C., Neumann, M., and Affolter, M. (2004). Genetic control of cell intercalation during tracheal morphogenesis in *Drosophila*. *Curr. Biol.* *14*, 2197–2207.
- Sadler, T.W. (1985). *Langman's Medical Embryology* (Baltimore: William & Wilkins).
- Schnatwinkel, C., Christoforidis, S., Lindsay, M.R., Uttenweiler-Joseph, S., Wilm, M., Parton, R.G., and Zerial, M. (2004). The Rab5 effector Rabankyrin-5 regulates and coordinates different endocytic mechanisms. *PLoS Biol.* *2*, E261.
- Shiga, Y., Tanaka-Matakatsu, M., and Hayashi, S. (1996). A nuclear GFP/ β -galactosidase fusion protein as a marker for morphogenesis in living *Drosophila*. *Dev. Growth Differ.* *38*, 99–106.
- Stenmark, H., Parton, R.G., Steele-Mortimer, O., Lutcke, A., Gruenberg, J., and Zerial, M. (1994). Inhibition of rab5 GTPase activity stimulates membrane fusion in endocytosis. *EMBO J.* *13*, 1287–1296.
- Swanson, J. (1989). Fluorescent labeling of endocytic compartments. *Methods Cell Biol.* *29*, 137–151.
- Swanson, L.E., and Beitel, G.J. (2006). Tubulogenesis: an inside job. *Curr. Biol.* *16*, R51–R53.
- Tepass, U., and Hartenstein, V. (1994). The development of cellular junctions in the *Drosophila* embryo. *Dev. Biol.* *161*, 563–596.
- Tonning, A., Hemphala, J., Tang, E., Nannmark, U., Samakovlis, C., and Uv, A. (2005). A transient luminal chitinous matrix is required to model epithelial tube diameter in the *Drosophila* trachea. *Dev. Cell* *9*, 423–430.
- Uv, A., Cantera, R., and Samakovlis, C. (2003). *Drosophila* tracheal morphogenesis: intricate cellular solutions to basic plumbing problems. *Trends Cell Biol.* *13*, 301–309.
- van der Bliek, A.M., and Meyerowitz, E.M. (1991). Dynamin-like protein encoded by the *Drosophila* shibire gene associated with vesicular traffic. *Nature* *351*, 411–414.
- Wang, S., Jayaram, S.A., Hemphala, J., Senti, K.A., Tsarouhas, V., Jin, H., and Samakovlis, C. (2006). Septate-junction-dependent luminal deposition of chitin deacetylases restricts tube elongation in the *Drosophila* trachea. *Curr. Biol.* *16*, 180–185.
- Wilhelm, J.E., Buszczak, M., and Sayles, S. (2005). Efficient protein trafficking requires trailer hitch, a component of a ribonucleoprotein complex localized to the ER in *Drosophila*. *Dev. Cell* *9*, 675–685.
- Wucherpfennig, T., Wilsch-Brauninger, M., and Gonzalez-Gaitan, M. (2003). Role of *Drosophila* Rab5 during endosomal trafficking at the synapse and evoked neurotransmitter release. *J. Cell Biol.* *161*, 609–624.
- Yamanushi, T., Hirata, A., Oka, T., and Nakano, A. (1996). Characterization of yeast *sar1* temperature-sensitive mutants, which are defective in protein transport from the endoplasmic reticulum. *J. Biochem. (Tokyo)* *120*, 452–458.
- Youson, J.H. (1984). Differentiation of the segmented tubular nephron and excretory duct during lamprey metamorphosis. *Anat. Embryol. (Berl.)* *169*, 275–292.
- Zhu, M.Y., Wilson, R., and Leptin, M. (2005). A screen for genes that influence fibroblast growth factor signal transduction in *Drosophila*. *Genetics* *170*, 767–777.